

Dark Glueball Direct Detection

Ji-Wei Li,^{1,*} Roman Pasechnik,^{2,†} Wei Wang,^{3,‡} and Zhi-Wei Wang^{1,§}

¹*School of Physics, The University of Electronic Science and Technology of China,
No. 2006, Xiyuan Ave, West Hi-Tech Zone, Chengdu, China*

²*Department of Physics, Lund University SE-223 62 Lund, Sweden*

³*State Key Laboratory of Dark Matter Physics, Key Laboratory for Particle Astrophysics and Cosmology (MOE),
Shanghai Key Laboratory for Particle Physics and Cosmology,
Shanghai Jiao Tong University, Shanghai 200240, China*

We consider glueball dark matter (DM) in a Yang-Mills dark sector confined at Λ_D scale and coupled to the Standard Model through electrically and dark-color charged vector-like fermion portals, with the mass scale m_ψ . In a simple case with two lightest mass-degenerate vector-like fermions with opposite electric charges the effective amplitudes with one C -odd glueball (oddball) and odd number of photons vanish, rendering the lightest C -odd spin-1 state with mass m_χ a viable DM candidate provided that $m_\psi \gtrsim 5.5\Lambda_D$. We develop a controlled effective field theory framework with non-perturbative information supported by QCD phenomenology leading to a quantitative prediction for coherent elastic glueball scattering off nuclei. We find a steep scaling of the spin-independent cross section $\sigma_{\text{SI}} \propto \Lambda_D^{2,15} m_\psi^{-8}$. This implies that the sensitivity of the current and next-generation xenon experiments in the range of $\sigma_{\text{SI}} \sim 10^{-46} - 10^{-48} \text{ cm}^2$ corresponds to $m_\psi \simeq 3 - 30 \text{ GeV}$, respectively, for $\Lambda_D \simeq 0.55 - 5.5 \text{ GeV}$. We provide a minimal UV completion of the portal sector compatible with collider phenomenology. Our results pave a quantitative foundation for testing glueball DM in direct-detection experiments.

I: Introduction.—The particle nature of dark matter (DM) remains unknown, and increasingly stringent bounds on weakly coupled candidates have strengthened the case for a richer hidden sector. Among many DM models, confining dark non-Abelian sectors provide a broadly motivated UV-complete framework for strongly interacting DM. As in QCD of the Standard Model (SM), confinement generates mass gap and naturally yields composite states – dark hadrons – governed by strong dynamics as reviewed in Ref. [1]. Such sectors can also feature sizable DM self-interactions that may affect small-scale structure while remaining compatible with current cosmological and astrophysical constraints [2, 3].

A systematic framework for secluded strong dynamics is provided by the “hidden valley” paradigm [4–6], which emphasizes that portals to a confining sector can yield complex hidden hadronization and, often, long-lived states with displaced decays [7]. In the minimal confining formulation, i.e. a pure Yang-Mills theory, the infrared spectrum consists of glueballs. Pure-gluon hidden valleys and their portal-induced decays were systematically explored in Refs. [8, 9], while the necessary nonperturbative inputs (glueball masses and matrix elements) are anchored by lattice determinations of the glueball spectrum [10, 11]. This “dark glueball” limit is thus theoretically clean yet phenomenologically rich: it is strongly coupled in the infrared, but admits controlled effective descriptions once matched to nonperturbative information.

Dark glueballs have long been explored as DM can-

didates. Early studies of hidden $SU(N)$ glueball DM [12, 13] established the cosmological picture, emphasizing number-changing reactions and dark-sector thermodynamics. In ultraviolet-motivated formulations, glueballs can be overproduced or decay too late (the “dark glueball problem” [14]), while nonstandard cosmologies can substantially reshape the viable parameter space [15]. Lattice-calibrated thermal EFTs further show that relic-density predictions are naturally tied to the confinement scale and the dark-to-visible temperature ratio, and can deviate significantly from conventional estimates [16, 17], motivating nonperturbative inputs throughout glueball phenomenology.

Confining dark sectors are amenable to multi-messenger probes. A first-order confinement transition may generate a stochastic gravitational-wave (GW) background [18, 19]. Using lattice-informed effective descriptions, dark $SU(N)$ Yang-Mills confinement and its implications for GW signals have been studied in [20–23]. Complementary sensitivity comes from indirect detection when DM annihilates into dark glueballs that subsequently decay to SM states [24], and from collider searches for exotic Higgs decays and long-lived signatures of dark confinement [25, 26]. Together, these channels motivate a unified program in which cosmology, astrophysics, and laboratory searches jointly probe strong hidden dynamics.

Direct detection remains the least developed part of the glueball-DM program: unlike pointlike DM, minimal portals induce high-dimensional couplings, and recoil rates require controlled matching from ultraviolet portals to nonperturbative glueball amplitudes. Photon-mediated scattering provides a generic route for neutral but polarizable composites [27, 28], while heavy-mediator portals can be organized within gluon/chromo-Rayleigh

* jiweili@std.uestc.edu.cn

† Corresponding: roman.pasechnik@fysik.lu.se

‡ wei.wang@sjtu.edu.cn

§ Corresponding: zhiwei.wang@uestc.edu.cn

EFTs [29, 30]. These encode the DM response in local operators, whereas for glueballs the scattering amplitude must be supplied nonperturbatively, and related dynamics can yield extremely suppressed electromagnetic couplings in other composite settings [31]. A key open question is whether glueball DM can be placed on a comparably quantitative footing for *direct* searches, with controlled matching between ultraviolet portals, nonperturbative glueball matrix elements, and experimentally relevant scattering amplitudes.

In this Letter, we address this question by adopting nonperturbative information from QCD phenomenology and establish a tensor-Pomeron-inspired EFT framework for direct detection. For electrically charged portal fermions with $m_\psi \gg \Lambda_D$ and C -odd glueballs below $2m_\psi$, integrating out the portal yields two-photon operators that control nuclear scattering via two off-shell (Coulomb) photons. We study two minimal benchmarks: a single charged fermion, and a two-flavor vector-like portal with approximate global $SU(2)_D$ and opposite electric charges, which suppresses odd-photon couplings and render lightest “oddball” glueballs effectively stable. By linking glueball lifetimes to direct-detection rates within a controlled EFT framework, our results pave a quantitative foundation for direct searches of glueball DM.

II: Light glueballs and fermionic portal.—In this work, we consider a generic dark $SU(N)$ gauge theory confining at a scale Λ_D . Its low-energy spectrum consists of glueballs denoted as χ , i.e. purely gluonic bound states characterized by their spin and discrete quantum numbers J^{PC} . We focus on the lowest-lying $J = 0, 1$ states summarized in Table I, together with their P, C assignments and characteristic masses.

To connect the dark glueball sector to the SM, we introduce electrically charged portal fermions with mass scale m_ψ and work in the hierarchical regime $m_\psi \gg \Lambda_D$, such that the lightest composite states remain glueballs (glueball states of interest lie below the portal-pair threshold $2m_\psi$). For most of this Letter we adopt a low-energy EFT viewpoint – dark Yang-Mills coupled to QED through loops of heavy charged fermions – and defer a concrete electroweak (EW) completion and collider constraints to Sec. V. We consider two minimal benchmark portal structures: (I) a single electrically charged Dirac fermion ψ , and (II) two mass-degenerate electrically charged Dirac fermions ψ_+ and ψ_- forming a doublet of an (approximately) conserved global $SU(2)_D$ dark-flavor symmetry, with opposite electric charges $Q_{\psi_+} = -Q_{\psi_-}$.

a. Scenario I (heavy portal). For a minimal single- ψ portal with sufficiently large $m_\psi \gtrsim 10$ TeV required by astrophysical bounds on decaying DM [32, 33], DM would be dominated by the lightest C -even scalar 0^{++} and pseudoscalar 0^{-+} glueballs. In this regime, the portal-induced photon couplings mediated by fermion-box loop are extremely suppressed, leading to a negligible elastic glueball-nucleus cross section, below 10^{-70} cm².

b. Scenario II (light portal). In the approximate $SU(2)_D$ doublet portal with vector-like $m_{\psi_+} \simeq m_{\psi_-} \equiv$

J^{PC}	Mass/ $m_{0^{++}}$	Decay operator	Scaling	Portal
0^{++}	1	$G^2 F^2$	$\alpha_D^2 \alpha^2 \Lambda_D^9 m_\psi^{-8}$	I
0^{-+}	~ 1.55	$G\tilde{G}F\tilde{F}$		
0^{+-}	~ 2.7	$G^3 F$	$\alpha_D^3 \alpha \Lambda_D^9 m_\psi^{-8}$	I/II
		$G^3 F^3$	$\alpha_D^3 \alpha^3 \Lambda_D^{17} m_\psi^{-16}$	
0^{--}	—	$\tilde{G}G^2 F$	$\alpha_D^3 \alpha \Lambda_D^9 m_\psi^{-8}$	
		$\tilde{G}G^2 \tilde{F}F^2$	$\alpha_D^3 \alpha^3 \Lambda_D^{17} m_\psi^{-16}$	
1^{++}	—	$G^3 F$	$\alpha_D^3 \alpha \Lambda_D^9 m_\psi^{-8}$	I/II ^a
1^{-+}	~ 2.49			
1^{+-}	~ 1.78	$G^3 F$	$\alpha_D^3 \alpha \Lambda_D^9 m_\psi^{-8}$	I/II
		$G^3 F^3$	$\alpha_D^3 \alpha^3 \Lambda_D^{17} m_\psi^{-16}$	
1^{--}	~ 2.44	$\tilde{G}G^2 F$	$\alpha_D^3 \alpha \Lambda_D^9 m_\psi^{-8}$	
		$\tilde{G}G^2 \tilde{F}F^2$	$\alpha_D^3 \alpha^3 \Lambda_D^{17} m_\psi^{-16}$	

TABLE I. Scenario I (“heavy portal”): $m_\psi \gtrsim 10$ TeV (unfavorable for direct detection). Scenario II (“light portal”): an approximately $SU(2)_D$ -symmetric *dark-flavor* doublet (ψ_+, ψ_-) with $m_{\psi_+} \simeq m_{\psi_-} \equiv m_\psi \lesssim \mathcal{O}(100$ GeV) and opposite electric charges $Q_{\psi_+} = -Q_{\psi_-}$. For case ^a, the glueball is stable for mass below $2m_e \sim 1$ MeV. Here, α_D and $\alpha \simeq 1/137$ denote dark $SU(N)$ and fine-structure couplings.

m_ψ and $Q_{\psi_+} = -Q_{\psi_-}$, the lightest 1^{+-} and next-to-lightest 1^{--} C -odd vector glueballs (oddballs) are (nearly) stable being viable DM candidates while heavier oddballs are expected to be Boltzmann suppressed. In the dark-flavor symmetry limit, any loop amplitude involving a single oddball and $2n + 1$ photons vanishes due to $Q_{\psi_+}^{2n+1} + Q_{\psi_-}^{2n+1} = 0$, forbidding radiative cascades such as $1^{+-}, 1^{--} \rightarrow 0^{++} + \gamma$. The elastic glueball-nucleus scattering would be dominated by the two-photon exchange which will be studied in detail below. For light portals, it is imperative to verify their consistency with collider constraints (Sec. V). Provided that 1^{+-} is heavier than 0^{++} , its relative abundance would be Boltzmann-suppressed, thus, mitigating its overproduction. The portal thermal history differs in the two scenarios mainly because of their large mass hierarchy. While in Scenario II the fermions annihilate away before confinement, in Scenario I a small residual $\psi\bar{\psi}$ population may survive down to $T \sim \Lambda_D$ but the corresponding bound states are short-lived.

Table I summarizes the lowest $J = 0, 1$ glueballs and their leading portal-induced couplings to photons scaling with $\alpha_D, \alpha, \Lambda_D$ and m_ψ and indicates which benchmark controls the late-time phenomenology. It also flags that the C -even vectors 1^{++} and 1^{-+} can be long-lived since the Landau-Yang theorem forbids $1^{++,-+} \rightarrow \gamma\gamma$, whereas in Scenario II the dominant decay mode $1^{+-,-+} \rightarrow \gamma(\gamma^* \rightarrow \ell^+ \ell^-)$ is forbidden below the threshold of $2m_e$.

Transitioning to direct detection, the portal-induced EFT operators in Table I also mediate scattering in matter. In the Coulomb regime, for either portal scenario, $\chi A \rightarrow \chi A$ proceeds via two off-shell photons and is governed by the doubly-virtual Compton tensor $T_{\mu\nu}^\chi$ from

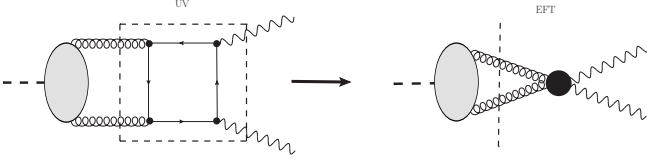


FIG. 1. UV-to-EFT matching for the effective two-photon-gluon vertex. The portal-fermion loop (left) is represented in the EFT as a dim-8 operator (right) that mediates both $\chi \rightarrow \gamma\gamma$ and χA elastic scattering via two off-shell photons.

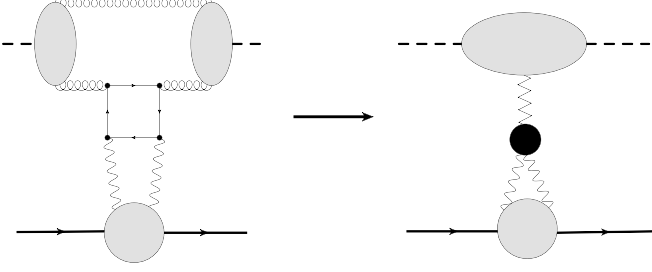


FIG. 2. Elastic glueball-nucleus scattering in the Coulomb regime. Left panel shows two-photon exchange mediated by portal-box, while right one illustrates the factorized form with the glueball Compton tensor $T_{\mu\nu}^{\chi}$, modeled as $T_{\mu\nu}^{\chi} \sim \Gamma(\gamma\gamma\mathbb{P}_D) \Delta \Gamma(\chi\chi\mathbb{P}_D)$ in the dark-Pomeron framework.

the dim-8 F^2G^2 matching (Fig. 1). We now compute this two-photon exchange for a generic glueball state $\chi(J^{PC})$, with $J = 0, 1$.

III: Elastic glueball scattering off a nucleus.— Consider elastic $\chi A \rightarrow \chi A$ scattering of a dark glueball state $\chi(J^{PC})$ off a nucleus A (mass number A , charge Z) at rest. We focus on the coherent Coulomb regime relevant for Galactic DM, $v_{\text{rel}} \sim 10^{-3}$, where the interaction is dominated by impact parameters $b \gtrsim R_A$ (equivalently, $|\mathbf{q}| \lesssim 1/R_A$) and is encoded by the nuclear form factor $\mathcal{F}_A(Q^2)$. At leading order in α , the process proceeds via exchange of two off-shell photons, Fig. 2. The glueball side is described by the doubly-virtual Compton tensor $T_{\mu\nu}^{\chi}$ for $\gamma^*(k_1)\chi(p) \rightarrow \gamma^*(k_2)\chi(p')$, generated by the portal-induced dim-8 operator schematically denoted F^2G^2 (see Table I). In fact, $T_{\mu\nu}^{\chi}$ factorizes into a short-distance matrix element $\gamma^*\gamma^* \rightarrow g_D g_D$ and a long-distance one, $\langle \chi | G^2 | \chi \rangle$. The full elastic amplitude $\chi(p)A(P) \rightarrow \chi(p')A(P')$ is written in terms of $T_{\mu\nu}^{\chi}$ as:

$$\mathcal{M}_{\chi} = (4\pi\alpha)^2 Z^2 \int \frac{d^4k}{(2\pi)^4} \frac{J_A^{\mu}(k_1) J_A^{\nu}(k_2) T_{\mu\nu}(p, q; k)}{(k_1^2 + i\epsilon)(k_2^2 + i\epsilon)}, \quad (1)$$

in terms $k \equiv (k_1 - k_2)/2$ the relative photon momentum, $q \equiv p' - p$ the total exchanged momentum in the t -channel, with $|\mathbf{q}| \simeq \sqrt{-t}$ and $q^0 \simeq -|\mathbf{q}|^2/(2m_A) \ll |\mathbf{q}|$, and J_A^{μ} the elastic current of a spinless nucleus (normalized to Z) defined as

$$J_A^{\mu}(k) \equiv \langle A(P') | J_{\text{em}}^{\mu}(0) | A(P) \rangle = (P+P')^{\mu} \mathcal{F}_A(Q^2), \quad (2)$$

with $Q^2 \equiv -k^2 > 0$ and $\mathcal{F}_A(0) = 1$. In the A rest frame,

$$J_A^{\mu}(k) \simeq (2m_A, \mathbf{0}) \mathcal{F}_A(Q^2), \quad (3)$$

so that the scattering is driven by exchanges of the longitudinally polarized virtual photons as expected in the Coulomb regime, while transverse components of J_A^{μ} are suppressed by $|\mathbf{q}|/m_A \ll 1$. Carrying out k^0 integral, one obtains

$$\mathcal{M}_{\chi} \simeq e^4 Z^2 (2m_A)^2 \int \frac{d^3\mathbf{k}}{(2\pi)^3} \mathcal{F}_A(\omega_1^2) \mathcal{F}_A(\omega_2^2) K \mathcal{C}_L, \quad (4)$$

$$K = \frac{1}{2\omega_1\omega_2} \frac{\omega_1 + \omega_2}{(\omega_1 + \omega_2)^2 - (q^0)^2}, \quad \mathcal{C}_L = T_{00}, \quad (5)$$

in terms of the photon energies $\omega_{1,2} \simeq |\mathbf{k}_{1,2}|$ and 3-momenta $\mathbf{k}_{1,2} \equiv \mathbf{q}/2 \pm \mathbf{k}$.

The elastic hadron scattering in QCD is dominated at high energies by the Pomeron \mathbb{P} exchange, which in the leading-log picture of perturbative QCD can be viewed as a color-singlet gluonic ladder, while at lower energies additional Reggeon (light $\psi\psi$) exchanges contribute. In the considered dark Yang-Mills sector, there are no light fermions (i.e. $m_{\psi} \gtrsim 5.5\Lambda_D$), so the analogous vacuum exchange is a purely gluonic “dark Pomeron” \mathbb{P}_D even at low energies (zigzag line in Fig. 2), which controls the forward regime of small momentum transfers, $|t| \lesssim \Lambda_D^2$; by contrast, t -channel exchange of the heavy portal fermions is suppressed.

In this forward limit, we evaluate the doubly-virtual Compton tensor $T_{\mu\nu}^{\chi}$ for $\gamma^*\chi \rightarrow \gamma^*\chi$ in the Ewerz–Maniatis–Nachtmann (EMN) framework, modeling it by exchange of a soft $C = +1$ spin-2 dark Pomeron \mathbb{P}_D . This parallels the EMN description of Compton scattering off pions ($J = 0$) and ρ mesons ($J = 1$) in QCD [34–36]. In the EMN model, $T_{\mu\nu}^{\chi}$ admits a factorized form in terms of a $\gamma\gamma\mathbb{P}_D$ vertex, the propagator Δ , and a $\chi\chi\mathbb{P}_D$ vertex, supplemented by an overall elastic slope factor. The \mathbb{P}_D propagator carries two symmetric index pairs and factorizes into the spin-2 projector $\mathcal{P}_{\kappa\lambda}^{\alpha\beta}$ and a scalar Regge factor $\mathcal{R}_D(W^2, t)$:

$$\Delta_{\kappa\lambda}^{\alpha\beta} = \mathcal{P}_{\kappa\lambda}^{\alpha\beta} \mathcal{R}_D = \mathcal{P}_{\kappa\lambda}^{\alpha\beta} \frac{(-iW^2\alpha'_D)^{\varepsilon_D + \alpha'_D t}}{W^2}, \quad (6)$$

$$\mathcal{P}_{\kappa\lambda}^{\alpha\beta} = \frac{1}{4} (g_{\kappa}^{\alpha} g_{\lambda}^{\beta} + g_{\kappa}^{\beta} g_{\lambda}^{\alpha} - \frac{1}{2} g_{\kappa\lambda} g^{\alpha\beta}), \quad W^2 = (p + k_1)^2.$$

with $\varepsilon_D [\text{GeV}^0]$ and $\alpha'_D [\text{GeV}^{-2}]$ the intercept parameters of the soft “dark Pomeron” trajectory that can be matched to their QCD counterparts ε, α' known from fits to soft (low- Q^2) QCD data (see Table II).

The effective $\gamma\gamma\mathbb{P}_D$ vertex can be written as

$$i\Gamma_{\mu\nu\kappa\lambda}^{(\gamma\gamma\mathbb{P}_D)} = 2a_D^{\gamma} \Gamma_{\mu\nu\kappa\lambda}^{(0)} - b_D^{\gamma} \Gamma_{\mu\nu\kappa\lambda}^{(2)}, \quad (7)$$

where $\Gamma^{(0)}$ and $\Gamma^{(2)}$ are the standard gauge-invariant EMN tensor structures (for on-shell photons they correspond to helicity-0 and helicity-2, respectively) [34–36], with a_D^{γ} and b_D^{γ} carrying mass dimensions [$a_D^{\gamma} = \text{GeV}^{-3}$ and $b_D^{\gamma} = \text{GeV}^{-1}$]. Gauge invariance implies

the Ward identities $k_1^\mu \Gamma_{\mu\nu\kappa\lambda}^{(\gamma\gamma\mathbb{P}_D)} = k_2^\nu \Gamma_{\mu\nu\kappa\lambda}^{(\gamma\gamma\mathbb{P}_D)} = 0$. The effective $\chi\chi\mathbb{P}_D$ vertex $\Gamma^{(\chi\chi\mathbb{P}_D)}$ has different structure for $\chi_{J=0} \equiv S$ and $\chi_{J=1} \equiv V$ dark glueballs, namely,

$$\begin{aligned} i\Gamma_{\alpha\beta}^{(SS\mathbb{P}_D)} &= -2i\beta_D^S \left[(p'+p)_\alpha (p'+p)_\beta - \frac{1}{4}g_{\alpha\beta} (p'+p)^2 \right], \\ i\Gamma_{\alpha\beta\rho\sigma}^{(VV\mathbb{P}_D)} &= 2a_D^V \Gamma_{\alpha\beta\rho\sigma}^{(0)} - b_D^V \Gamma_{\alpha\beta\rho\sigma}^{(2)}, \end{aligned} \quad (8)$$

where $\Gamma^{(0,2)}$ denote the same gauge-invariant tensor basis with the obvious replacement $(\mu, \nu, k_1, k_2) \rightarrow (\rho, \sigma, p, p')$, while β_D^S [GeV $^{-1}$] and a_D^V [GeV $^{-3}$], b_D^V [GeV $^{-1}$] are the dark Pomeron couplings to the S - and V -glueballs, respectively. The final ingredient of the amplitude is the elastic form factor, $F_{el} = \exp[-b_{\text{eff}}^D |t|/2]$, with the effective slope parameter b_{eff}^D [GeV $^{-2}$] absorbing the exponential slopes of $\chi\chi\mathbb{P}_D$ and $\gamma\gamma\mathbb{P}_D$ vertices. Combining the above elements, the resulting Compton subprocess amplitudes for S - and V -glueballs are found as

$$T_{\mu\nu}^S = F_{el} \Gamma_{\mu\nu\kappa\lambda}^{(\gamma\gamma\mathbb{P}_D)} \Delta^{\kappa\lambda\alpha\beta} \Gamma_{\alpha\beta}^{(SS\mathbb{P}_D)}. \quad (9)$$

$$T_{\mu\nu, \lambda\lambda'}^V = F_{el} \Gamma_{\mu\nu\kappa\lambda}^{(\gamma\gamma\mathbb{P}_D)} \Delta^{\kappa\lambda\alpha\beta} \Gamma_{\alpha\beta\rho\sigma}^{(VV\mathbb{P}_D)} \varepsilon_\lambda^\rho \varepsilon_{\lambda'}^\sigma, \quad (10)$$

where $\varepsilon_\lambda^\rho(p)$ and $\varepsilon_{\lambda'}^\sigma(p')$ ($\lambda, \lambda' = 0, \pm 1$) are the polarization vectors of the initial and final V -glueball states.

For concreteness, we focus on dark SU(3) and rescale key QCD inputs (e.g. the constituent-quark mass $m_q \simeq \Lambda$ and the QCD confinement scale Λ) to their dark-sector counterparts. Using naive dimensional analysis, we then map the Pomeron intercept, effective couplings, and elastic-slope parameter extracted from Deep Inelastic Scattering (DIS) fits [35] onto the corresponding dark-Pomeron parameters summarized in Table II.

SU(3) $_D$	ϵ_D	α'_D	β_D^S	b_{eff}^D	a_D^V	b_D^V	a_D^γ	b_D^γ
QCD	0.09	0.25	1.76	5.0	2.34	4.22	0.08	0.4
SU(3) $_D$ QCD	1.0	$\frac{\Lambda^2}{\Lambda_D^2}$	$\frac{\Lambda}{\Lambda_D}$	$\frac{\Lambda^2}{\Lambda_D^2}$	$\frac{0.6\Lambda}{m_V^2 \Lambda_D}$	$\frac{\Lambda}{\Lambda_D}$	$\frac{m_q^4 \alpha_D^\psi \Lambda_D}{m_\psi^4 \alpha_s^* \Lambda}$	$\frac{m_q^4 \alpha_D^\psi \Lambda_D^3}{m_\psi^4 \alpha_s^* \Lambda^3}$

TABLE II. The QCD Pomeron parameters and their rescaling factors to that of the dark Pomeron \mathbb{P}_D . In the case of QCD, we take the $\mathbb{P}SS$ coupling equal to $\beta_{\pi\pi\mathbb{P}}$ of the pion-Pomeron $\pi\pi\mathbb{P}$ vertex and $\mathbb{P}VV$ couplings equal to those of ρ -meson $-a_{\rho\rho\mathbb{P}}$ and $b_{\rho\rho\mathbb{P}}$. The latter satisfy the relation $2m_\rho^2 a_{\rho\rho\mathbb{P}} + b_{\rho\rho\mathbb{P}} = 4\beta_{\pi\pi\mathbb{P}}$ and have been estimated using the ratio of the corresponding f_2 (or a_2) meson couplings to ρ found in Ref. [34], $b_{\rho\rho f_2}/a_{\rho\rho f_2} \simeq 3m_\rho^2$. In practical calculations, we take $\alpha_s^* \equiv \alpha_s(\Lambda) \simeq 0.5$ and $\alpha_D^\psi \equiv \alpha_D(m_\psi) \simeq 0.12$.

IV: Direct detection cross section.—Starting from the Coulomb two-photon amplitude in Eq. (4), the elastic differential spin-independent (SI) scattering cross section off a nucleus A in nonrelativistic regime is found as

$$\frac{d\sigma_{\text{el}}}{dt} = \frac{|\mathcal{M}_\chi(s, t)|^2}{16\pi \lambda(s, m_A^2, m_\chi^2)}, \quad \lambda \xrightarrow{\text{NR}} 4m_A^2 m_\chi^2 v_{\text{rel}}^2, \quad (11)$$

Here, $s = (p + P)^2$, $t \simeq -\mathbf{q}^2 = -2m_A T_A$ with $T_A \ll m_{A, \chi}$ the nuclear recoil energy, and $\lambda(x, y, z) = x^2 + y^2 +$

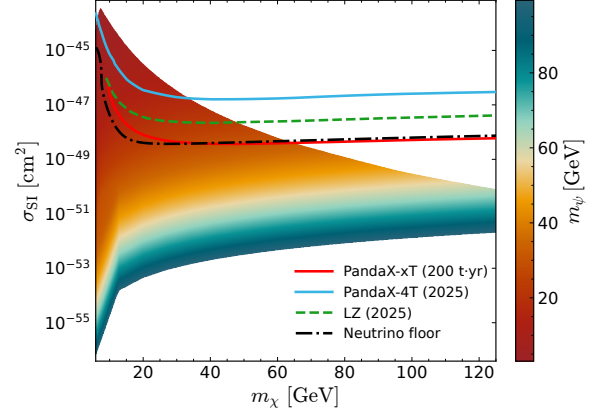


FIG. 3. Spin-independent (SI) per-nucleon cross section for glueball DM in the Coulomb regime compared to bounds from Xenon experiments. The colored domain spans over the portal-fermion mass m_ψ , in the color bar, and the odd-ball mass m_χ satisfying the glueball stability $m_\chi < 2m_\psi$. Projected detector sensitivities are given for PandaX-xT [37], PandaX-4T and LZ [38, 39] with the neutrino floor [40].

$z^2 - 2xy - 2xz - 2yz$ the Källén function. To compare with experimental limits we quote the conventional per-nucleon normalization,

$$\sigma_{\text{SI}} \equiv \frac{\mu_{\chi p}^2}{\mu_{\chi A}^2} \frac{1}{A^2} \int_{t_{\text{min}}}^0 dt \frac{d\sigma_{\text{el}}}{dt}, \quad t_{\text{min}} \simeq -4\mu_{\chi A}^2 v_{\text{rel}}^2, \quad (12)$$

with $\mu_{\chi A}$ and $\mu_{\chi p}$ the DM-nucleus and DM-proton reduced masses. Evaluating \mathcal{M}_χ in Eq. (4), we obtain the predicted $\sigma_{\text{SI}}(m_\chi)$ shown in Fig. 3 for different portal mass scale m_ψ in the color bar, together with the current and projected bounds from Xenon-based experiments. As was discussed before, the applicability of the glueball EFT in our analysis is justified in the heavy portal mass limit $m_\psi \gg \Lambda_D$ while in practice it suffices to consider $m_\psi > 5.5\Lambda_D$ following from the glueball stability condition. Numerically, we find a steep parametric scaling $\sigma_{\text{SI}} \propto \Lambda_D^{2.15} m_\psi^{-8}$. To be within the current PandaX sensitivity, for instance, one needs a sufficiently light portal, $m_\psi \lesssim 20$ GeV, while PandaX-T can extend the reach up to $m_\psi \sim 30$ GeV. Note, that the lowest $\Lambda_D^{\text{min}} \simeq 0.55$ GeV follows from the minimal Xenon recoil energy set to $T_{\text{Xe}}^{\text{min}} = 0.5$ keV, while the maximal recoil energy $T_{\text{Xe}}^{\text{max}} = 2\mu_{\chi A}^2 v_{\text{rel}}^2/m_A$ is set by DM kinetic energy.

V: Electroweak completion and constraints.—The observability of glueball DM via direct-detection motivates a light charged dark-colored portal state with mass $m_\psi \lesssim 20$ GeV. We impose the inclusive LEP1 Z -width constraint [41], LEP2 single-/multi-photon searches [42, 43], LHC Higgs-width limits from coupling fits [44, 45], and oblique-parameter bounds [46–49].

A minimal EW completion introduces two vector-like $SU(2)_L$ -singlet fermions U, D with $U(1)_Y$ hypercharges $Y = \pm 1/2$ and two vector-like $SU(2)_L$ -doublet fermions

Ψ_U, Ψ_D with $Y = 0$, while Higgs-width limits are controlled by an additional *scalar* doublet Φ (2HDM-like scenario) together with a Z_2 symmetry (see Appendix A for more details). In a *split-mixing* pattern, the light ψ_{\pm} mass-eigenstates originate from different singlet-doublet blocks in the mass matrix. The inclusive Z -width bound enforces a narrow Z -phobic window,

$$g_V^{\text{eff}}(\psi_{\pm}) = \mp s_W^2 \pm \frac{1}{2}f, \quad \Delta\Gamma_Z(Z \rightarrow \psi_{\pm}\bar{\psi}_{\pm}) \lesssim 2.3 \text{ MeV},$$

where 2.3 MeV is the experimental uncertainty on the total Z width at LEP1 [41], and $f \equiv \sin^2\theta$ is the doublet fraction of the light mass-eigenstates ψ_{\pm} . This implies $f \in [0.394, 0.532]$ for $m_{\psi} \simeq 20$ GeV. Moreover, in the split-mixing completion the light states ψ_+ and ψ_- originate from different $SU(2)_L$ doublets, so the gauge vertex $W_{\mu}\bar{\psi}_+\gamma^{\mu}\psi_-$ is absent already such that $\Delta\Gamma_W^{\text{tree}}(W \rightarrow \psi_+\bar{\psi}_-) = 0$ at tree level making it easier to satisfy the LEP bound, $\Delta\Gamma_W \lesssim 0.10$ GeV [50, 51], due to suppressed radiative corrections. Besides, there are heavier Dirac partners X^{\pm} which do not affect LEP phenomenology for $m_X \gtrsim 105$ GeV. On the other hand, the singlet–doublet mixing required by the Z -phobic window breaks custodial symmetry and yields a positive fermionic shift ΔT_{ferm} , so X^{\pm} cannot be arbitrarily decoupled from the EW scale. Global EW fits typically require $T \lesssim 0.2$ at 95% CL, within the correlated (S, T) ellipse [46–49]. A negative scalar contribution $\Delta T_{\text{scal}} < 0$ from the 2HDM spectrum can reduce total T well below 0.2; see Appendix A.

At LEP2 the irreducible production is $e^+e^- \rightarrow \gamma^*/Z^* \rightarrow \psi_{\pm}\bar{\psi}_{\pm}$. Since the produced pair forms a confined (neutral ρ -meson-like) bound state, the visible signature is therefore governed by its subsequent glueball cascade and radiative $0^{++} \rightarrow \gamma\gamma$ decays in the final state. Hence, the LEP2 sensitivity depends on the 0^{++} decay length with three potential cases – prompt, displaced and monophoton + missing energy ones [42, 43]. Using the scaling of dim-8 effective operator with the (lightest) portal mass, we get

$$c\tau_{0^{++}} \simeq 0.3 \text{ m} \left(\frac{m_{\psi}}{80 \text{ GeV}} \right)^8 \left(\frac{10 \text{ GeV}}{\Lambda_D} \right)^9. \quad (13)$$

Our benchmark result $c\tau_{0^{++}} \simeq 5.8 \text{ cm}$ lies in the displaced window which often is the hardest to constrain. It can further evade both the standard prompt and missing-energy searches.

Finally, the Higgs-width constraint is implemented by requiring the exotic rate to obey $\Gamma(h \rightarrow \psi\bar{\psi}) \leq \Gamma_h^{\text{SM}} \text{BR}_{\text{BSM}}^{\text{max}}$, with $\text{BR}_{\text{BSM}}^{\text{max}} \simeq 0.107$ from the LHC Higgs coupling fits [44, 45]. As shown in Appendix A, this is ensured by *sequestering* of the portal Yukawa coupling into a second Higgs doublet Φ , which acquires the vacuum expectation value (vev) v_{Φ} and features a small CP-even mixing θ_s to the observed Higgs state. An example of a benchmark scenario that satisfies the phenomenological bounds above is given in Table III.

VI: Discussion and conclusions.—We have shown that C -odd vector glueball (oddball) DM from a con-

$\Delta\Gamma_Z$	$\Delta\Gamma_W$	$c\tau_{0^{++}}$	T_{ferm}	$\text{BR}_{\text{BSM}}(h)$
$\lesssim 2.3 \text{ MeV}$	$\lesssim 0.10 \text{ GeV}$	$1 \text{ mm} - 1 \text{ m}$	$\lesssim 0.2$	< 0.107
2.30 MeV	0	5.8 cm	0.18	0.088

TABLE III. Experimental bounds (top row) and corresponding predictions (bottom row) for our EW-complete model benchmark point: $m_{\psi} = 20$ GeV, $f = 0.394$, $m_X \simeq 119$ GeV, $\Lambda_D = 3.5$ GeV, and $v_{\Phi} = 30$ GeV, $\theta_s = 2.5 \times 10^{-3}$.

fining dark Yang-Mills sector can be confronted with direct-detection data in a controlled EFT framework. To demonstrate the power of our framework, we designed a minimal phenomenologically consistent formulation of light Dirac portal sector, which (i) ensures stability of oddball DM, and (ii) its accessibility at current and future direct-detection experiments. The major novelty of our EFT framework is the modeling of the oddball-nucleus scattering via two-photon exchange using the dark tensor-Pomeron approach inspired by QCD. This has been achieved by a consistent EFT matching of the basic nonperturbative elements to those known from QCD phenomenology. As the main result, we find that the spin-independent cross section scales as $\sigma_{\text{SI}} \propto \Lambda_D^{2.15} m_{\psi}^{-8}$ with the portal mass $m_{\psi} \gtrsim 5.5\Lambda_D$ and the dark confinement scale Λ_D . This result naturally delineates an essentially invisible multi-TeV-portal regime and a light-portal window $m_{\psi} \simeq 3 - 30$ GeV for $\Lambda_D \simeq 0.55 - 5.5$ GeV potentially testable at current and next-generation Xenon-based facilities. By constructing a minimal electroweak completion for such a light portal sector, we demonstrate its consistency with collider phenomenology. Our results provide a compact bridge from UV portals to nuclear recoil spectra paving a quantitative foundation for direct detection tests of confining dark sectors.

Acknowledgments.— We warmly thank Jianglei Liu, Ning Zhou and Shaofeng Ge for fruitful discussions. Z.-W.W. is supported in part by the National Natural Science Foundation of China (Grant No. 12475105). W.W. is supported in part by the Natural Science Foundation of China under grants No. 12125503 and 12305103.

Appendix A: Electroweak Dirac portal model

1. Field content and charges

We introduce two vector-like $SU(2)_L$ singlets and two vector-like $SU(2)_L$ doublets,

$$U \sim (1, Y = +1/2), \quad (A1)$$

$$D \sim (1, Y = -1/2), \quad (A2)$$

$$\Psi_U = \begin{pmatrix} \psi_{U+} \\ \psi_{U-} \end{pmatrix} \sim (2, Y = 0), \quad (A3)$$

$$\Psi_D = \begin{pmatrix} \psi_{D+} \\ \psi_{D-} \end{pmatrix} \sim (2, Y = 0). \quad (A4)$$

	H	Φ	Ψ_U	Ψ_D	U	D
Z_2	+	-	+	-	-	+

TABLE IV. A single Z_2 choice that simultaneously (i) sequesters the portal Yukawa from the SM Higgs and (ii) forbids cross-sector couplings, making the split-mixing structure radiatively stable. SM fields are taken Z_2 -even.

Electric charge is $Q = T_3 + Y$, so $Q(U) = +1/2$, $Q(D) = -1/2$, and $Q(\psi_{U\pm}) = Q(\psi_{D\pm}) = \pm 1/2$. After EWSB, $U(1)_{\text{em}}$ remains unbroken, hence the charged-fermion mass matrix is block-diagonal in fixed- Q sectors.

2. Sequestered portal doublet and a Z_2 symmetry

Besides the SM Higgs doublet H , we introduce an additional scalar doublet Φ ,

$$H^T = \left(G^+, \frac{v + h_0 + iG^0}{\sqrt{2}} \right), \quad (\text{A5})$$

$$\Phi^T = \left(\phi^+, \frac{v_\Phi + \varphi + ia}{\sqrt{2}} \right). \quad (\text{A6})$$

To forbid direct portal Yukawas to H while allowing Yukawas to Φ , we impose a discrete symmetry in Table IV. Then $\bar{\Psi}_{U,D}\tilde{H}U$ and $\bar{\Psi}_{U,D}HD$ are forbidden, but the portal Yukawas to Φ (below) are allowed. A soft Z_2 -breaking term in the scalar potential,

$$V(H, \Phi) \supset m_{12}^2 H^\dagger \Phi + \text{h.c.}, \quad (\text{A7})$$

induces a small CP-even mixing between h_0 and φ , parameterized by an angle θ_s .

3. Split-mixing Yukawa sector in components

The gauge-invariant portal Yukawas are

$$\mathcal{L}_Y^{\text{portal}} \supset -y_U \bar{\Psi}_U \tilde{\Phi} U - y_D \bar{\Psi}_D \Phi D + \text{h.c.}, \quad (\text{A8})$$

where $\tilde{\Phi} \equiv i\sigma_2 \Phi^*$. Using (A6),

$$\tilde{\Phi} = \begin{pmatrix} \frac{v_\Phi + \varphi - ia}{\sqrt{2}} \\ -\phi^- \end{pmatrix}, \quad (\text{A9})$$

so that (A8) expands as

$$-y_U \bar{\Psi}_U \tilde{\Phi} U = -\frac{y_U}{\sqrt{2}} (v_\Phi + \varphi - ia) \bar{\psi}_{U+} U + y_U \bar{\psi}_{U-} \phi^- U, \quad (\text{A10})$$

$$-y_D \bar{\Psi}_D \Phi D = -\frac{y_D}{\sqrt{2}} (v_\Phi + \varphi + ia) \bar{\psi}_{D-} D - y_D \bar{\psi}_{D+} \phi^+ D. \quad (\text{A11})$$

Only the neutral vev v_Φ generates mass mixing, and it appears *only* in $\bar{\psi}_{U+}U$ and $\bar{\psi}_{D-}D$. Thus, in the split-mixing pattern, the components ψ_{U-} and ψ_{D+} do not mix at tree level.

Defining the EWSB-induced mixing masses

$$\delta_U \equiv \frac{y_U v_\Phi}{\sqrt{2}}, \quad \delta_D \equiv \frac{y_D v_\Phi}{\sqrt{2}}, \quad (\text{A12})$$

we obtain two independent 2×2 mixing blocks in the $Q = \pm 1/2$ sectors.

4. Charged-sector mass Lagrangian and diagonalization

Including vector-like masses M_U, M_D and singlet masses m_U, m_D , the charged-sector mass terms read

$$\begin{aligned} \mathcal{L}_{\text{mass}} = & -(\bar{U}_L \ \bar{\psi}_{U+}^L) M_+ \begin{pmatrix} U_R \\ \psi_{U+}^R \end{pmatrix} - (\bar{D}_L \ \bar{\psi}_{D-}^L) M_- \begin{pmatrix} D_R \\ \psi_{D-}^R \end{pmatrix} + \text{h.c.} \\ & - M_U \bar{\psi}_{U-} \psi_{U-} - M_D \bar{\psi}_{D+} \psi_{D+}, \end{aligned} \quad (\text{A13})$$

with

$$M_+ = \begin{pmatrix} m_U & \delta_U \\ \delta_U & M_U \end{pmatrix}, \quad M_- = \begin{pmatrix} m_D & \delta_D \\ \delta_D & M_D \end{pmatrix}. \quad (\text{A14})$$

Each block is diagonalized by an orthogonal rotation. Defining $c_\pm \equiv \cos \theta_\pm$ and $s_\pm \equiv \sin \theta_\pm$,

$$\begin{pmatrix} U \\ \psi_{U+} \end{pmatrix} = \begin{pmatrix} c_+ & -s_+ \\ s_+ & c_+ \end{pmatrix} \begin{pmatrix} \psi^+ \\ X^+ \end{pmatrix}, \quad (\text{A15})$$

$$\begin{pmatrix} D \\ \psi_{D-} \end{pmatrix} = \begin{pmatrix} c_- & -s_- \\ s_- & c_- \end{pmatrix} \begin{pmatrix} \psi^- \\ X^- \end{pmatrix}. \quad (\text{A16})$$

The light eigenstates are

$$\psi_+ = c_+ U + s_+ \psi_{U+}, \quad \psi_- = c_- D + s_- \psi_{D-}. \quad (\text{A17})$$

The mixing angles satisfy

$$\tan 2\theta_+ = \frac{2\delta_U}{M_U - m_U}, \quad \tan 2\theta_- = \frac{2\delta_D}{M_D - m_D}, \quad (\text{A18})$$

and we define the doublet fractions $f_{\pm} \equiv s_{\pm}^2$ (in the symmetric benchmark $f_+ = f_- \equiv f$).

The corresponding eigenvalues are

$$m_{\psi_+} = \frac{m_U + M_U}{2} - \sqrt{\left(\frac{M_U - m_U}{2}\right)^2 + \delta_U^2}, \quad (\text{A19})$$

$$m_{X^+} = \frac{m_U + M_U}{2} + \sqrt{\left(\frac{M_U - m_U}{2}\right)^2 + \delta_U^2}, \quad (\text{A20})$$

$$m_{\psi_-} = \frac{m_D + M_D}{2} - \sqrt{\left(\frac{M_D - m_D}{2}\right)^2 + \delta_D^2}, \quad (\text{A21})$$

$$m_{X^-} = \frac{m_D + M_D}{2} + \sqrt{\left(\frac{M_D - m_D}{2}\right)^2 + \delta_D^2}. \quad (\text{A22})$$

Comment on the W-width. The vanishing of the light–light charged current in split mixing follows from the gauge structure:

$$\mathcal{L}_W \supset \frac{g}{\sqrt{2}} W_{\mu}^+ \left(\bar{\psi}_{U+} \gamma^{\mu} \psi_{U-} + \bar{\psi}_{D+} \gamma^{\mu} \psi_{D-} \right) + \text{h.c.}, \quad (\text{A23})$$

which couples only within each doublet. Since ψ_+ contains ψ_{U+} while ψ_- contains ψ_{D-} [cf. (A17)], there is no tree-level $W\psi_+\psi_-$ vertex, hence $\Delta\Gamma_W^{\text{tree}}(W \rightarrow \psi_+\bar{\psi}_-) = 0$ independently of whether the mixing masses $\delta_{U,D}$ originate from H or from Φ .

5. Scalar mixing and suppressed Higgs coupling to light portals

The CP-even fields (h_0, φ) mix into mass eigenstates (h, h') via

$$\begin{pmatrix} h \\ h' \end{pmatrix} = \begin{pmatrix} \cos \theta_s & \sin \theta_s \\ -\sin \theta_s & \cos \theta_s \end{pmatrix} \begin{pmatrix} h_0 \\ \varphi \end{pmatrix}, \quad |\theta_s| \ll 1, \quad (\text{A24})$$

so $\varphi = h \sin \theta_s + h' \cos \theta_s$. Because the portal Yukawas are sequestered into Φ (A8), only φ couples directly to the portal fermions.

From (A10)–(A11), the CP-even interaction in the gauge basis can be written as

$$\begin{aligned} \mathcal{L} \supset & -\frac{y_U}{\sqrt{2}} \varphi \bar{\psi}_{U+} U - \frac{y_D}{\sqrt{2}} \varphi \bar{\psi}_{D-} D + \text{h.c.} \\ & = -\frac{\varphi}{v_{\Phi}} \left(\delta_U \bar{\psi}_{U+} U + \delta_D \bar{\psi}_{D-} D \right) + \text{h.c.} \end{aligned} \quad (\text{A25})$$

Rotating to the fermion mass basis (A15)–(A16), the diagonal couplings to the light eigenstates are

$$g_{\varphi\psi_+\psi_+} = \frac{\delta_U}{v_{\Phi}} \sin 2\theta_+, \quad g_{\varphi\psi_-\psi_-} = \frac{\delta_D}{v_{\Phi}} \sin 2\theta_-. \quad (\text{A26})$$

Finally, inserting $\varphi = h \sin \theta_s + \dots$ from (A24) into (A25) yields

$$g_{h\psi\psi} = \sin \theta_s g_{\varphi\psi_+\psi_+} \simeq \left(\frac{\delta_{U,D}}{v_{\Phi}} \sin 2\theta_{\pm} \right) \sin \theta_s, \quad (\text{A27})$$

which explains the relation $g_{h\psi\psi} = g_{\varphi\psi\psi} \sin \theta_s$ used in the main text. Here, we utilize the symmetric benchmark suggested by mass-degeneracy of the lightest eigenstates, with $g_{h\psi\psi} \equiv g_{h\psi_+\psi_+} = g_{h\psi_-\psi_-}$, $m_U = m_D$, $M_U = M_D \equiv M$, $\delta_U = \delta_D \equiv \delta$, and $\theta_+ = \theta_- \equiv \theta$. Then, the partial width (per Dirac fermion) is

$$\Gamma(h \rightarrow \psi_{\pm} \bar{\psi}_{\pm}) = N \frac{g_{h\psi\psi}^2 m_h}{8\pi} \beta_h^3, \quad (\text{A28})$$

where $m_h \simeq 125$ GeV is the SM Higgs boson mass, N is the number of dark colors, and

$$\beta_h \equiv \sqrt{1 - \frac{4m_{\psi}^2}{m_h^2}}.$$

In this case, the exotic Higgs width into the two light charged states reads $\Gamma_{\text{BSM}}(h) \simeq 2\Gamma(h \rightarrow \psi_+\bar{\psi}_+)$.

6. Oblique parameters: scalar contribution

The scalar doublet Φ contains a charged state $H^{\pm} \equiv \phi^{\pm}$, a CP-odd state $A \equiv a$, and a mostly- Φ CP-even state which we denote by φ (mass m_{φ}) in the small-mixing limit $|\theta_s| \ll 1$. We denote their masses as $(m_{H^{\pm}}, m_A, m_{\varphi})$.

For completeness we write the leading one-loop scalar contributions to the oblique parameters (in the inert/sequestered limit) as

$$\begin{aligned} \Delta T_{\text{scal}} &= \frac{1}{32\pi s_W^2 m_W^2} \left[F(m_{H^{\pm}}, m_A) + F(m_{H^{\pm}}, m_{\varphi}) \right. \\ &\quad \left. - F(m_A, m_{\varphi}) \right], \end{aligned} \quad (\text{A29})$$

$$\Delta S_{\text{scal}} \simeq \frac{1}{12\pi} \ln \frac{m_{\varphi}^2}{m_A^2}. \quad (\text{A30})$$

Here, F is the standard finite Veltman function,

$$F(m_1, m_2) = m_1^2 + m_2^2 - \frac{2m_1^2 m_2^2}{m_1^2 - m_2^2} \ln \frac{m_1^2}{m_2^2}. \quad (\text{A31})$$

A spectrum with $m_A < m_{H^{\pm}} < m_{\varphi}$ yields $\Delta T_{\text{scal}} < 0$ and can partially (or fully) compensate the positive fermionic shift ΔT_{ferm} . For fixed physical scalar masses, ΔS_{scal} and ΔT_{scal} are essentially independent of the CP-even mixing angle θ_s , which instead controls the Higgs-width sequestering discussed above.

- [1] G. D. Kribs and E. T. Neil, *Review of strongly-coupled composite dark matter models and lattice simulations*, *Int. J. Mod. Phys. A* **31** (2016) 1643004 [1604.04627].
- [2] D. N. Spergel and P. J. Steinhardt, *Observational evidence for self-interacting cold dark matter*, *Phys. Rev. Lett.* **84** (2000) 3760 [astro-ph/9909386].
- [3] S. Tulin and H.-B. Yu, *Dark matter self-interactions and small scale structure*, *Phys. Rept.* **730** (2018) 1 [1705.02358].
- [4] M. J. Strassler and K. M. Zurek, *Echoes of a hidden valley at hadron colliders*, *Phys. Lett. B* **651** (2007) 374 [hep-ph/0604261].
- [5] M. J. Strassler, *Possible effects of a hidden valley on supersymmetric phenomenology*, hep-ph/0607160.
- [6] T. Han, Z. Si, K. M. Zurek and M. J. Strassler, *Phenomenology of hidden valleys at hadron colliders*, *JHEP* **07** (2008) 008 [0712.2041].
- [7] M. J. Strassler and K. M. Zurek, *Discovering the higgs through highly-displaced vertices*, *Phys. Lett. B* **661** (2008) 263 [hep-ph/0605193].
- [8] J. E. Juknevich, D. Melnikov and M. J. Strassler, *A pure-gluon hidden valley i. states and decays*, *JHEP* **07** (2009) 055 [0903.0883].
- [9] J. E. Juknevich, *Pure-gluon hidden valleys through the higgs portal*, *JHEP* **08** (2010) 121 [0911.5616].
- [10] C. J. Morningstar and M. Peardon, *The glueball spectrum from an anisotropic lattice study*, *Phys. Rev. D* **60** (1999) 034509 [hep-lat/9901004].
- [11] Y. Chen et al., *Glueball spectrum and matrix elements on anisotropic lattices*, *Phys. Rev. D* **73** (2006) 014516 [hep-lat/0510074].
- [12] A. Soni and Y. Zhang, *Hidden $SU(n)$ glueball dark matter*, *Phys. Rev. D* **93** (2016) 115025 [1602.00714].
- [13] L. Forestell, D. E. Morrissey and K. Sigurdson, *Non-abelian dark forces and the relic densities of dark glueballs*, *Phys. Rev. D* **95** (2017) 015032 [1605.08048].
- [14] J. Halverson, B. D. Nelson and F. Ruehle, *String theory and the dark glueball problem*, *Phys. Rev. D* **95** (2017) 043527 [1609.02151].
- [15] B. S. Acharya, M. Fairbairn and E. Hardy, *Glueball dark matter in non-standard cosmologies*, *JHEP* **07** (2017) 100 [1704.01804].
- [16] P. Carenza, R. Pasechnik, G. Salinas and Z.-W. Wang, *Glueball dark matter revisited*, *Phys. Rev. Lett.* **129** (2022) 261302 [2207.13716].
- [17] P. Carenza, T. Ferreira, R. Pasechnik and Z.-W. Wang, *Glueball dark matter, precisely*, *Phys. Rev. D* **108** (2023) 123027 [2306.09510].
- [18] C. Caprini et al., *Science with the space-based interferometer elisa. ii: Gravitational waves from cosmological phase transitions*, *JCAP* **04** (2016) 001 [1512.06239].
- [19] P. Schwaller, *Gravitational waves from a dark phase transition*, *Phys. Rev. Lett.* **115** (2015) 181101 [1504.07263].
- [20] W.-C. Huang, M. Reichert, F. Sannino and Z.-W. Wang, *Testing the dark $SU(n)$ yang-mills theory confined landscape: From the lattice to gravitational waves*, *Phys. Rev. D* **104** (2021) 035005 [2012.11614].
- [21] M. Reichert, F. Sannino, Z.-W. Wang and C. Zhang, *Dark confinement and chiral phase transitions: gravitational waves vs matter representations*, *JHEP* **01** (2022) 003 [2109.11552].
- [22] Z. Kang, J. Zhu and S. Matsuzaki, *Dark confinement-deconfinement phase transition: a roadmap from Polyakov loop models to gravitational waves*, *JHEP* **09** (2021) 060 [2101.03795].
- [23] R. Pasechnik, M. Reichert, F. Sannino and Z.-W. Wang, *Gravitational waves from composite dark sectors*, *JHEP* **02** (2024) 159 [2309.16755].
- [24] D. Curtin and C. Gemmill, *Indirect detection of dark matter annihilating into dark glueballs*, *JHEP* **09** (2023) 010 [2211.05794].
- [25] D. Curtin and C. B. Verhaaren, *Discovering uncolored naturalness in exotic higgs decays*, *JHEP* **12** (2015) 072 [1506.06141].
- [26] A. Batz, T. Cohen, D. Curtin, C. Gemmill and G. D. Kribs, *Dark sector glueballs at the LHC*, *JHEP* **04** (2024) 070 [2310.13731].
- [27] N. Weiner and I. Yavin, *How dark are majorana WIMPs? signals from midm and rayleigh dark matter*, *Phys. Rev. D* **86** (2012) 075021 [1206.2910].
- [28] G. Ovanessian and L. Vecchi, *Direct detection of dark matter polarizability*, *JHEP* **07** (2015) 128 [1410.0601].
- [29] R. M. Godbole, G. Mendiratta and T. M. Tait, *A simplified model for dark matter interacting primarily with gluons*, **1506.01408**.
- [30] Y. Bai and J. Osborne, *Chromo-rayleigh interactions of dark matter*, *JHEP* **09** (2015) 054 [1506.07110].
- [31] P. Carenza, R. Pasechnik and Z.-W. Wang, *Composite heavy axionlike dark matter*, *Phys. Rev. Lett.* **135** (2025) 021001.
- [32] C. Blanco and D. Hooper, *Constraints on Decaying Dark Matter from the Isotropic Gamma-Ray Background*, *JCAP* **03** (2019) 019 [1811.05988].
- [33] P. Munbodh and S. Profumo, *Astrophysical constraints from synchrotron emission on very massive decaying dark matter*, *Phys. Rev. D* **110** (2024) 043014 [2405.00798].
- [34] C. Ewerz, M. Maniatis and O. Nachtmann, *A Model for Soft High-Energy Scattering: Tensor Pomeron and Vector Odderon*, *Annals Phys.* **342** (2014) 31 [1309.3478].
- [35] D. Britzger, C. Ewerz, S. Glazov, O. Nachtmann and S. Schmitt, *The Tensor Pomeron and Low- x Deep Inelastic Scattering*, *Phys. Rev. D* **100** (2019) 114007 [1901.08524].
- [36] P. Lebiedowicz, O. Nachtmann and A. Szczurek, *Deeply virtual Compton scattering in the tensor-pomeron approach*, *Phys. Lett. B* **835** (2022) 137497 [2208.12693].
- [37] PANDA-X, PANDAX Collaboration, A. Abdukerim et al., *PandaX-xT—A deep underground multi-ten-tonne liquid xenon observatory*, *Sci. China Phys. Mech. Astron.* **68** (2025) 221011 [2402.03596].
- [38] PANDAX Collaboration, Z. Bo et al., *Dark Matter Search Results from 1.54 Tonne-Year Exposure of PandaX-4T*, *Phys. Rev. Lett.* **134** (2025) 011805 [2408.00664].
- [39] LZ Collaboration, J. Aalbers et al., *Dark Matter Search Results from 4.2 Tonne-Years of Exposure of the LUX-ZEPLIN (LZ) Experiment*, *Phys. Rev. Lett.* **135**

- (2025) 011802 [2410.17036].
- [40] C. A. J. O'Hare, *New Definition of the Neutrino Floor for Direct Dark Matter Searches*, *Phys. Rev. Lett.* **127** (2021) 251802 [2109.03116].
- [41] ALEPH, DELPHI, L3, OPAL, SLD, LEP ELECTROWEAK WORKING GROUP, SLD ELECTROWEAK GROUP, SLD HEAVY FLAVOUR GROUP Collaboration, S. Schael et al., *Precision electroweak measurements on the Z resonance*, *Phys. Rept.* **427** (2006) 257 [hep-ex/0509008].
- [42] OPAL Collaboration, *Photonic events with missing energy in e^+e^- collisions at $\sqrt{s} = 189$, GeV*, *Eur. Phys. J. C* **18** (2000) 253 [hep-ex/0005002].
- [43] L3 Collaboration, *Single- and multi-photon events with missing energy in e^+e^- collisions at LEP*, *Phys. Lett. B* **587** (2004) 16 [hep-ex/0402002].
- [44] ATLAS Collaboration and CMS Collaboration, *Measurements of the Higgs boson production and decay rates and constraints on its couplings from a combined ATLAS and CMS analysis of the LHC pp collision data at $\sqrt{s} = 7$ and 8 TeV*, *JHEP* **08** (2016) 045 [1606.02266].
- [45] ATLAS Collaboration, *Combination of searches for invisible decays of the Higgs boson using 139 fb^{-1} of proton-proton collision data at $\sqrt{s} = 13$ TeV collected with the ATLAS experiment*, *Physics Letters B* **842** (2023) 137963 [2301.10731].
- [46] Particle Data Group, *Review of Particle Physics (2025 update)*, <https://pdg.lbl.gov/2025/>, 2025. Online update of S. Navas et al. (Particle Data Group), *Phys. Rev. D* 110, 030001 (2024). Accessed 2026-02-04.
- [47] ALEPH Collaboration and DELPHI Collaboration and L3 Collaboration and OPAL Collaboration and LEP Electroweak Working Group, *Electroweak measurements in electron-positron collisions at W-boson-pair energies at LEP*, *Phys. Rept.* **532** (2013) 119 [1302.3415].
- [48] M. E. Peskin and T. Takeuchi, *A New constraint on a strongly interacting Higgs sector*, *Phys. Rev. Lett.* **65** (1990) 964.
- [49] M. E. Peskin and T. Takeuchi, *Estimation of oblique electroweak corrections*, *Phys. Rev. D* **46** (1992) 381.
- [50] P. D. Group, *Review of particle physics: W-boson width (2025 update)*, Particle listings (online PDF), 2025. See [rpp2025-list-w-boson.pdf](#).
- [51] S. Schael et al., *Electroweak measurements in electron-positron collisions at w-boson-pair energies at lep*, *Phys. Rept.* **532** (2013) 119 [1302.3415].